JOURNAL OF GEOPHYSICAL RESEARCH, VOL. 113, A00A03, doi:10.1029/2008JA013130, 2008

Remote measurements of ion temperatures in the terrestrial magnetotail

Amy M. Keesee,[1] Earl Scime,[1] and Mark B. Moldwin[2]

Received 27 February 2008; revised 31 March 2008; accepted 15 April 2008; published 30 July 2008.

[1] Time-resolved remote ion temperature measurements of the magnetosphere from 10 R_E to −60 R_E are presented for the first 48 h of the storm of 4–7 October 2000. Ion temperatures are calculated from Maxwellian fits to data from the Medium Energetic Neutral Atom instrument aboard the Imager for Magnetopause-to-Aurora Global Exploration spacecraft. The calculated ion temperatures in the magnetotail are consistent with in situ measurements from multiple geosynchronous spacecraft and Geotail at $x = -9$ R_E. The measurements indicate two separate instances of an earthward propagating increase in ion temperature during the storm. Ion heating is observed coincident with substorm injections at 0600 UT and 1720 UT on 4 October. At −12 R_E, the remotely measured ion temperatures are consistent with predictions of a solar wind velocity correlation equation only when the solar wind–magnetospheric coupling is strong. At other times, the measured ion temperature is 2–3 times larger than the predicted value.

Citation: Keesee, A. M., E. Scime, and M. B. Moldwin (2008), Remote measurements of ion temperatures in the terrestrial magnetotail, *J. Geophys. Res.*, *113*, A00A03, doi:10.1029/2008JA013130.

1. Introduction

[2] Two fundamental questions in magnetospheric physics are where and when substorms begin in the magnetotail. Simultaneous, multispacecraft measurements in the magnetotail, such as are being provided by the THEMIS mission, are likely to significantly improve our understanding of substorm processes in the magnetotail. Time-resolved remote measurements of the ion temperature throughout the entire magnetotail can also provide detailed information about plasma heating and the propagation of energetic ions in the magnetotail. Of particular relevance to substorm processes is the possible heating or energization of the magnetotail plasma in the range of 20–30 R_E downtail, the average location assumed for the near-Earth neutral line [*Nagai et al.*, 1998].

[3] Through model-based inversions of energetic neutral atom (ENA) image data from the Imager for Magnetopause-to-Aurora Global Exploration (IMAGE) spacecraft (see *Burch* [2000] for a review of the IMAGE spacecraft), ion distribution functions in the ring current and inner magnetosphere have been obtained for a number of magnetospheric events from 2000 to 2006 [*Brandt et al.*, 2002, 2003; *Zhang et al.*, 2005]. Direct fitting of ENA energy spectra from the Medium Energetic Neutral Atom (MENA) imager aboard IMAGE has also been shown to yield remotely determined ion temperatures consistent with locally measured values for the inner magnetosphere [*Scime et al.*, 2002].

[4] ENA studies of the magnetotail, however, are problematic. ENA fluxes from the magnetotail are much smaller than from the inner magnetosphere and are typically restricted to energies below a few tens of keV. Although crude models for estimating ENA fluxes from the magnetotail were constructed at the beginning of ENA instrument development [*Moore et al.*, 1994], to the best of our knowledge, no physics-based models have been developed for analysis of actual ENA fluxes from the magnetotail.

[5] Yet magnetotail ENA imaging is possible. *McComas et al.* [2002] demonstrated that during intense storm times, ENA fluxes from as far as tens of R_E down the magnetotail could be detected by MENA. Prior to a storm, plasma sheet loading occurs; reaching a maximum during the storm. *McComas et al.* [2002] showed that the best times to measure magnetotail ENA fluxes are just before and during major magnetospheric storms.

[6] In this work, we present ENA flux-derived ion temperatures as a function of distance from Earth for the first 2 d of the major geomagnetic storm of 4–7 October 2000. The ion temperatures were obtained by direct fits of the ENA energy spectra. The 4–7 October 2000 storm had a minimum Dst of −182 nT and was caused by multiple CMEs [*Zhang et al.*, 2003]. On the basis of analysis of the storm with the WINDMI model, *Horton et al.* [2005] concluded that the intervals of periodic substorm activity on 3 October and 4 October were not driven by fluctuations in the solar wind. *Brandt et al.* [2002, 2003] studied two of the substorms that occurred on 4 October using ENA images from the HENA instrument on the IMAGE satellite. The HENA data presented extended to $x = -14$ R_E. They measured a decrease in ring current associated ENA flux on

[1]Department of Physics, West Virginia University, Morgantown, West Virginia, USA.
[2]Institute of Geophysics and Planetary Physics, University of California, Los Angeles, California, USA.

0148-0227/08/2008JA013130$09.00

the tail side that they associated with earthward acceleration of ions by substorm electric fields. They also concluded that the observed increase in ring current energy was due to increased convection driven by the solar wind rather than proton injections resulting from the substorms.

2. Magnetotail Ion Temperatures

[7] A number of studies have reported ion temperatures in the magnetotail using single point, in situ measurements. Using ISEE-2 and ISEE-3 data, *Borovsky et al.* [1998] found a strong correlation between the solar wind velocity and ion temperature in the plasma sheet, for $-17.5\ R_E < x < -22.5\ R_E$ (GSM coordinates) and at geosynchronous orbit. Using Geotail ion measurements in the central plasma sheet for $-10\ R_E > x > -50\ R_E$ during magnetospherically quiet times, *Tsyganenko and Mukai* [2003] found that the ion temperature, typically ~5–10 keV for $-10\ R_E < x < -12\ R_E$, decreases tailward and is peaked at the midnight meridian. They also found that magnetotail ion temperatures increased with solar wind speed and southward B_z. During active intervals, *Baumjohann et al.* [1996] showed that ions in the central plasma sheet are heated by approximately 2 keV during the substorm expansion phase. This heating is more rapid in storm time substorms and yields an average magnetotail ion temperature of 8 keV. The heated ions are then transported earthward at speeds as high as 120 km/s. Multiple substorms during a magnetic storm can produce even higher ion temperatures in the central plasma sheet [*Baumjohann et al.*, 2003]. In a more recent Geotail study, *Nosé et al.* [2005] also found a strong, ion-mass-dependent correlation between the solar wind speed and the plasma sheet ion temperature for $-8.5\ R_E < x < -10.5\ R_E$.

[8] The mechanism of ion heating in the magnetotail is not fully understood. Two-dimensional hybrid simulations suggest that considerable parallel ion heating can occur in the plasma sheet boundary layer as a result of magnetotail reconnection [*Lin and Swift*, 1996]. Therefore, spatially localized ion heating could be used as an indicator of ongoing magnetic reconnection. On the other hand, *Hoshino* [2005] suggests that magnetotail ion heating is due to 2-D quasi-adiabatic compression perpendicular to the magnetic field during storms. On the basis of particle-in-cell (PIC) code results, *Lui* [2005] proposed that the ion heating is due to the cross-field current instability associated with substorms. Still other researchers have suggested mechanisms such as nonadiabatic heating by pitch angle scattering [*Liu and Rostoker*, 1995]; convection of heated plasma from the deep tail toward the inner magnetosphere due to magnetic field dipolarization during storms [*Kamide et al.*, 1998]; and conversion of the electric potential drop into ion energy after turbulent driven reductions in the z-component of the magnetotail magnetic field [*Taktakishvili et al.*, 2001].

[9] The ion temperature itself can play an important role in the dynamics of the magnetotail. Using a model of reconnection-driven magnetic turbulence based on Geotail measurements, *Veltri et al.* [1998] found that the increase in current sheet thickness is correlated with an increase in magnetotail ion temperature and not simply ion density. They also determined that the ion temperature gradient is important in balancing the outer magnetic pressure, suggesting that the current sheet is thick, in contrast to the Harris model of a thin current sheet. This implies that magnetic turbulence converts the ion acceleration due to the electric field into thermal motion and that the ion pressure dominates the current sheet. Thus, understanding the temperature and flow of magnetotail ions is critical to improving our understanding of reconnection in the magnetotail.

3. Experimental Results

[10] Since the details of the MENA instrument [*Pollock et al.*, 2000] and the remote ion temperature determination procedure have been described in detail elsewhere [*Scime et al.*, 2002; *Zaniewski et al.*, 2006], only a brief outline of the instrumentation and the analysis method is provided here. The MENA instrument is a time-of-flight (TOF) resolving, imaging ENA camera. Single-event data were used in this study, so the full TOF and angle information were available for each ENA count. A detailed model of the instrument response [*Henderson et al.*, 2005] was used to accurately sort the data into spin angle, polar angle, and TOF bins. The angle bins are referenced to the local spacecraft coordinate system which is aligned with the spacecraft-Earth line for each acquisition.

[11] To map the measured ENA fluxes to the terrestrial magnetosphere, a satellite look vector for each ENA imaging pixel is calculated based on the satellite's position in GSM coordinates (the x axis points toward the Sun and the z axis points along the northern magnetic pole in GSM). For each pixel in an ENA image, the intersection of the look vector with the GSM xy-plane is calculated and the ENA flux assigned to the appropriate xy-plane pixel. Using the same method as *McComas et al.* [2002] to improve the signal-to-noise of magnetotail ENA data, the fluxes mapped to all y positions (ranging from approximately $-60\ R_E < y < 60\ R_E$) for a particular x position are summed together to create a 1-D array of flux versus x position (ranging from approximately $-60\ R_E < x < 60\ R_E$). The ion temperatures at each downtail location are then calculated by correcting the ENA energy spectra for the known energy dependent charge-exchange cross sections, assuming the MENA data are dominated by the hottest plasma along each line-of-sight, and assuming a Maxwellian parent ion distribution [*Scime et al.*, 2002]. A sample fit to the corrected ENA flux versus energy bin is shown in Figure 1. As shown previously [*Zaniewski et al.*, 2006], oxygen neutrals misidentified as hydrogen neutrals by the MENA instrument have little to no effect on the ion temperature determination. Therefore, the increase in magnetospheric oxygen ion density during a storm can be neglected in this analysis.

[12] Although using fluxes from such a large y extent decreased the intrinsic spatial resolution of the measurements, it provided enough ENA counts for reliable ion temperature fits. The majority of the ENA fluxes originated from $-24\ R_E < y < 24\ R_E$, and limiting the fits to this region yielded ion temperature values that differed from those obtained from fits to the full y extent by less than 0.5 keV. For three different x axis locations averaged over DOY 278, 2000–2040 UT, we examined the ion temperatures obtained by fitting the flux values for five different ranges of y axis locations: the full $\pm 60\ R_E$, $\pm 24\ R_E$, 0 to 25 R_E, 0 to $-25\ R_E$, and $\pm 7.5\ R_E$. The ENA counts versus y axis location of the third energy bin (centered at 9.0 keV) for the three

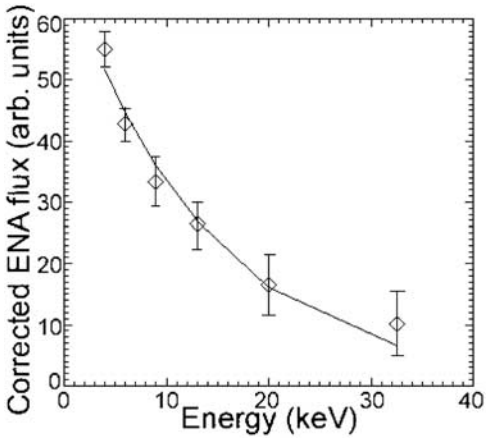

Figure 1. Energetic neutral atom (ENA) flux corrected by the energy dependent charge-exchange cross sections versus energy bin (diamonds) and the corresponding Maxwellian fit used to obtain the ion temperature.

x axis locations are shown in Figure 2, along with five bars indicating the five different ranges of y axis locations. Although considerably larger ENA fluxes are available in the low-energy bins, the poor statistics of the 40-min-averaged, 9.0 keV fluxes shown in Figure 2 highlight the need to include a large spatial extent along the y axis to obtain sufficient counts in the higher-energy bins for an accurate Maxwellian fit. The ion temperatures determined for each of the downtail locations and y axis ranges are shown in Table 1. For the two x axis locations that are furthest downtail, the standard deviations in the calculated ion temperatures are less than 1.3 keV For the x axis location closest to the Earth, $-4.5\ R_E > x > -7.5\ R_E$, the standard deviation in the ion temperature values was also 1.3 keV, but the fluxes in the lowest-energy bin had to be excluded to obtain reasonable fits for two of the subsets of the full y axis region. Essentially, the ENA statistics for those limited y regions were too small, again emphasizing the need to trade spatial resolution for improved statistics in this type of investigation.

[13] In this study, we have limited our analysis to $x < 10\ R_E$ because ENA imaging upstream of the magnetopause is not possible with MENA. The MENA instrument is unable to detect the sub-keV ENAs that are created by charge-exchange of the magnetosheath [*Russell*, 1990] and solar wind (OMNIWeb) plasma with background neutrals. Consequently, the hotter, denser plasma in the magnetosphere dominates the ENA fluxes obtained for lines of sight that pass through the magnetosphere and intersect the xy-plane upstream of the magnetopause.

[14] Since all the ENA fluxes are line-of-sight integrated, to confirm that our downstream ion temperatures are an accurate representation of ion temperatures in the xy-plane, we have compared our remote ion temperature measurements with in situ measurements from multiple spacecraft and with predictive models. Looking downtail, the hottest plasma population is most likely to be the central plasma sheet [*Hughes*, 1995]. The spatial resolution along the x axis is determined by where the lines of sight of each MENA imaging pixel intersect the outermost boundaries (along z) of the central plasma sheet. The thickness of the central plasma sheet is largest near the Earth and decreases further downtail, with a half-width range of $\sim 1-3\ R_E$ [*Kaufmann et al.*, 2001]. When IMAGE is at $x = -5\ R_E$ and $z = 5\ R_E$, the uncertainty in mapped location for lines of sight that intersect the x axis at $0 \geq x \geq -10\ R_E$ is less than 3 R_E. However, at $x = -60\ R_E$, the uncertainty grows to 11 R_E. In other words, direct mapping of ENA fluxes to the xy plane in GSM coordinates is inherently an uncertain process for a thick central plasma sheet and extremely long lines of sight. Therefore, in this study we have binned ENA fluxes mapped to the xy-plane into 3 R_E bins as a compromise between the good spatial resolution available in the inner magnetosphere and the poor spatial resolution available in the deep magnetotail.

[15] The calculated ion temperatures as a function of time and distance are shown in Figure 3a. The pixels along the time (horizontal) axis are 40-min averages of MENA data and the spatially resolved bins have been combined into 3 R_E bins along the distance (vertical) axis. Ion temperatures are shown for the sunward (up to 10 R_E) and antisunward directions. The maximum uncertainties in the ion temperatures from the Maxwellian fits for each temporal interval in Figure 3a were ±3 keV, ±2 keV, ±1 keV, and ±1 keV, respectively. Thus, for the first two intervals, the errors in the ion temperatures result from uncertainty in the Maxwellian fits. For the second two intervals (which had better statistics), the uncertainties in the ion temperature values appear to arise from the large range of y positions over which the ENA fluxes were summed (see Table 1). The IMF B_z obtained from ACE, lagged by 1 h, is also shown in Figure 3a. The hourly D_{st} index is shown in Figure 3b. A plot of the inverted AL geomagnetic index for 4 October 2000 is shown in Figure 4. Figure 5a shows an expanded region (see section 4) of Figure 3a that has increased temporal and spatial resolution. For Figure 5a, 20-min

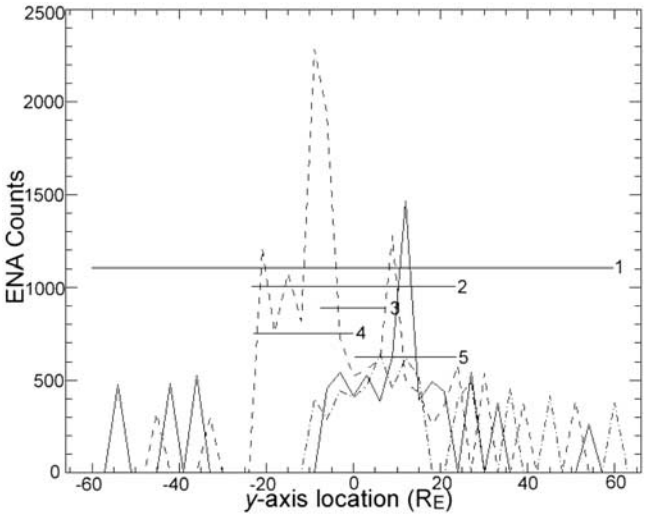

Figure 2. The ENA counts during 40 min versus y axis location of the third energy bin (centered at 9.0 keV) for x axis bins with data from $-4.5\ R_E > x > -7.5\ R_E$ (dashed line), $-10.5\ R_E > x > -13.5\ R_E$ (solid line), and $-16.5\ R_E > x > -19.5\ R_E$ (dash-dotted line). The numbered bars indicate the ranges of y axis locations used for the temperature fits shown in Table 1.

Table 1. Comparison of Temperatures Obtained From the Maxwellian Fit Using Five Ranges of y Axis Locations as Shown in Figure 2[a]

x Axis Values for Data Bin to Be Fit	1: $\|y\| < 60\ R_E$	2: $\|y\| < 24\ R_E$	3: $\|y\| < 7.5\ R_E$	4: $-25\ R_E < y < 0\ R_E$	5:0 $R_E < y < 25\ R_E$
$-4.5\ R_E > x > -7.5\ R_E$	4.4	4.4	7.2[b]	8.8	5.9[b]
$-10.5\ R_E > x > -13.5\ R_E$	6.4	6.6	7.3	7.2	6.5
$-16.5\ R_E > x > -19.5\ R_E$	9.8	8.9	8.0	6.9	10.1

[a]Temperature comparison is measured in keV. The comparison is done for three bins along the x axis.
[b]The lowest energy bin was suppressed to obtain a fit.

averages of MENA data have been mapped into 1 R_E bins for Day 278, 0500–1120 UT and $-15\ R_E < x < 5\ R_E$. Figure 5b (adapted from *Brandt et al.* [2002]) shows how the MENA lines of sight cross the magnetic field lines for a dipole field and for the Tsyganenko-96 [*Tsyganenko and Stern*, 1996] model.

[16] For comparison with our remotely determined values, single point, in situ, ion temperature measurements during this storm are available from a number of sources. Perpendicular ion temperatures from four multiple particle analyzer (MPA) instruments [*Bame et al.*, 1993] in geosynchronous orbit are shown in Figure 6 for intervals during which the satellites were within $y = \pm 2\ R_E$ of the x axis and $x < 0$. Also shown in Figure 6 (solid line) are the remote ion temperature values from Figure 3a that correspond to the geosynchronous location of the MPA instruments. The error bars shown for each interval in Figure 6 indicate the largest estimated error for that interval for all spatial locations and all times. Thus, the errors bars correspond to a conservative upper bound on the error in each remote ion temperature measurement for each interval. An estimate in the errors for the ion temperature measured by the MPA instruments has not been calculated (M. Thomsen, private communication, 2008). A similar comparison with ion temperature data from Geotail, when Geotail was within a few R_E of the x axis at $x = -9\ R_E$, is shown in Figure 7. The orbital paths for these satellites and IMAGE are shown in Figure 8. During this storm interval, there were no satellites capable of determining the local ion temperature, further downtail than $x = -9\ R_E$, and within $\pm 2\ R_E$ of the x axis.

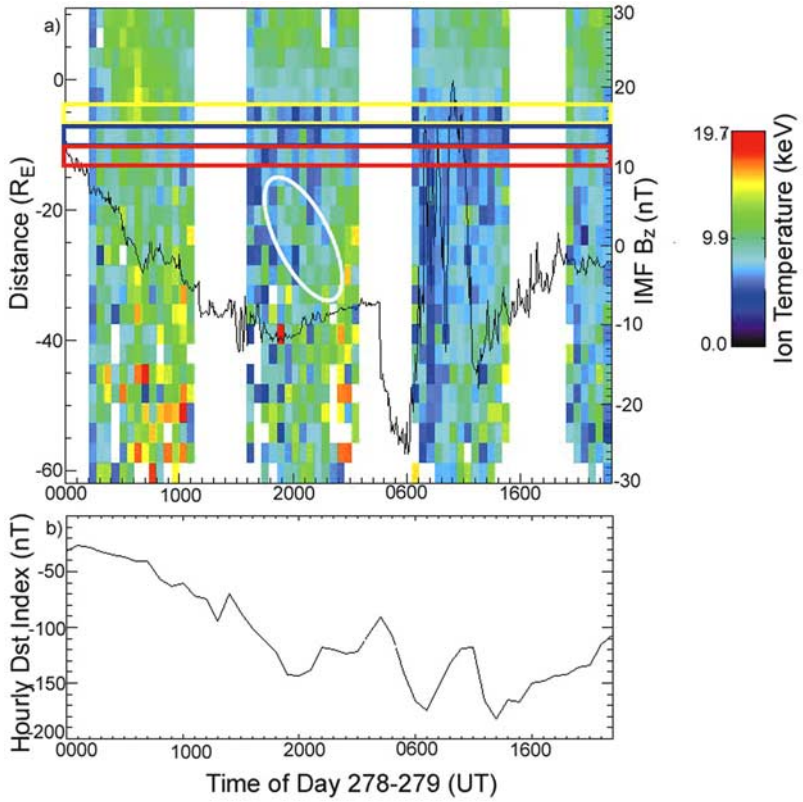

Figure 3. (a) Ion temperatures calculated from Medium Energetic Neutral Atom (MENA) data as a function of time and distance from the Earth. The pixels along the x axis (time) are 40 min averages of MENA data, and they are combined into 3 R_E bins along the y axis (distance). The IMF B_z measured by ACE, lagged by 1 h, is also shown. (b) Hourly D_{st} index. The data spans 4–5 October (278–279) 2000. The rows of data used for temperature comparisons (below) are indicated by the yellow (Figure 6), blue (Figure 7), and red (Figure 9) boxes. The white oval indicates a region of increased ion temperature that appears to propagate tailward.

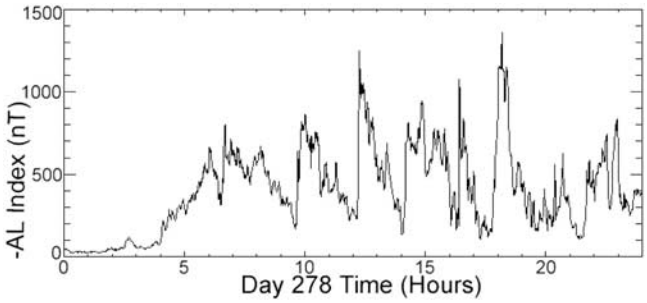

Figure 4. Inverted AL index for 4 October 2000.

[17] We have also compared our ion temperatures to those calculated for $x = -12\ R_E$ using the *Borovsky et al.* [1998] solar wind velocity scaling (Figure 9)

$$kT(t)[keV] = -3.65 + 0.019V_{sw}(t - 3hr), \quad (1)$$

where V_{sw} is the solar wind velocity measured by the ACE satellite. This equation is used in the simulations of *Fok et al.* [2003] to define a Maxwellian distribution at the $-12\ R_E$ nightside boundary. The simulation results were then used to interpret HENA measurements for this storm (http://mcf.gsfc.nasa.gov/IMAGE/storms/2000_278/).

4. Discussion

[18] As shown in the first interval of Figure 3a, (Day 278, 0200–1120 UT), during the main phase of the storm, there is significant ion heating throughout the magnetosphere. Such ion heating is consistent in magnitude and storm phase correlation with the ion heating seen in the superposed epoch analysis of 40 storms described by *Zaniewski et al.* [2006]. These remote measurements provide a unique perspective on transient and spatially localized ion heating events in the magnetosphere.

[19] For example, a region of intense ion heating within 5 R_E of the Earth at 0600 UT can be seen in Figure 3a that correlates with the onset of periodic substorm activity as demonstrated by peaks in the geomagnetic AL index (see Figure 4), proton and electron flux injection measurements observed by geosynchronous spacecraft [*Horton et al.*, 2005], and auroral onsets observed by the far ultraviolet (FUV) imager aboard IMAGE [*Brandt et al.*, 2002]. For lines of sight that map to this region, the hottest ions are likely in the horns of the plasma sheet, the narrow, high-

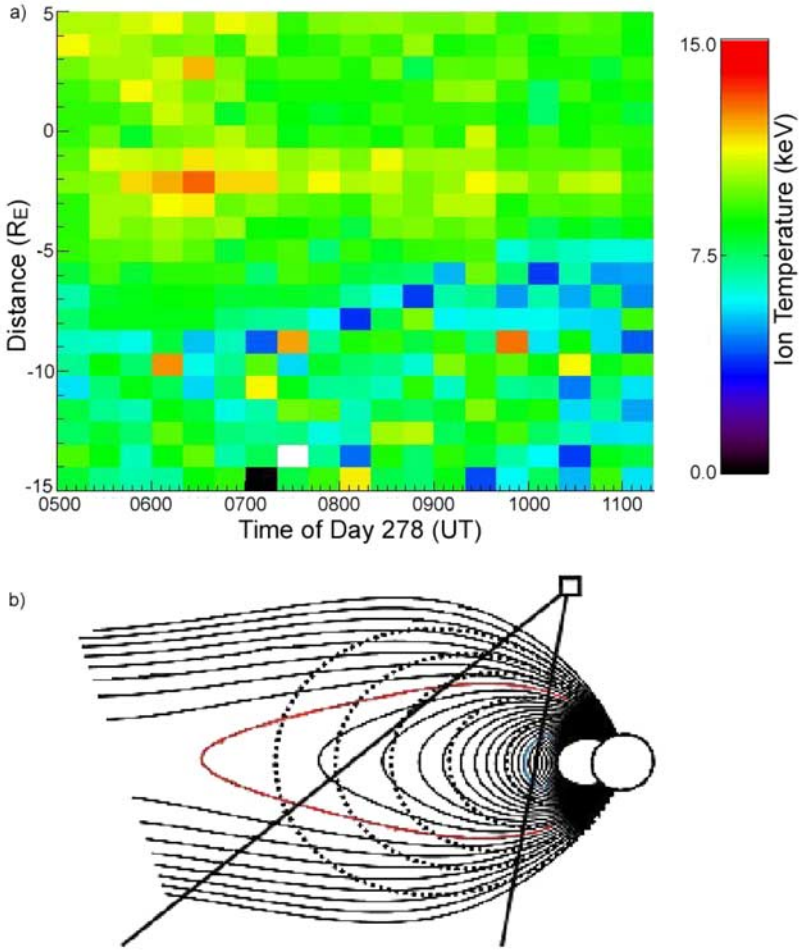

Figure 5. (a) Similar to Figure 3a, except the pixels along the x axis are 20 min averages of MENA data, and they are combined into 1 R_E bins along the y axis. (b) MENA lines of sight in relation to the magnetic field. Dipole field lines (dashed) for L = 4, 6, 8, 10, and 12 and field lines from the Tsyganenko-96 model (solid) are shown (adapted from *Brandt et al.* [2002]).

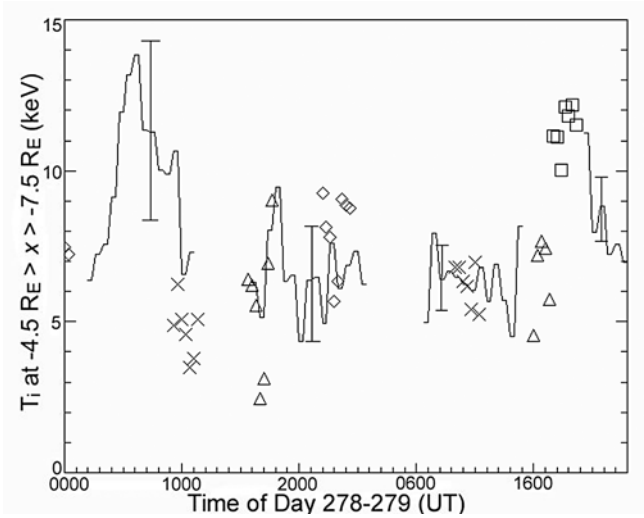

Figure 6. Ion temperatures calculated from MENA data (solid line) and measured by multiple particle analyzer (MPA) instruments on LANL geosynchronous satellites 1989 (crosses), 1991 (diamonds), 1994 (triangles), and 1997 (squares). Characteristic error bars are shown for each time interval from Figure 3a. The row of temperatures used is indicated in Figure 3a by the yellow box and corresponds to data taken at $-4.5\ R_E > x > -7.5\ R_E$.

latitude extensions of the plasma sheet to the ionosphere [*Suszcynsky et al.*, 1993]. In the enhanced view of this region (Figure 5a), we see that the heating begins at 0520 UT from an initial ion temperature of ~10 keV, increasing to a maximum of 12.8 keV at 0620 UT (the same time as the sharp dip in the inverted AL index shown in Figure 4), and then decreases to the surrounding ion temperature of ~10 keV at 0720 UT. An ion temperature increase of ~2–3 keV is consistent with the finding of *Baumjohann et al.* [1996] during a substorm expansion phase, though the maximum ion temperature found here is higher than their maximum temperature of 8 keV. Figure 5b shows the magnetic field line geometry of the magnetotail as viewed by MENA, including both the dipole field lines (dashed) and the field lines based on the Tsyganenko-96 model (solid). When looking from MENA toward the *xy*-plane within a few R_E of the Earth, the line of sight crosses through the horn of the plasma sheet which contains magnetic field lines that intersect the *xy*-plane at a range of *x* axis values. Thus, the high temperatures in Figure 5a could be ions trapped at high magnetic latitude, for example on the red field line, that intersects the *xy*-plane much further from the Earth than where the line of sight maps. However, if the hot ions seen in Figure 5a were from the red field line, we would expect to see a band of high temperatures along *x* from additional lines of sight passing through the plasma along that field line, as shown in Figure 5b. Because the high ion temperatures are spatially localized, we believe that the hot ions are from a field line at a much lower magnetic latitude, such as the blue field line in Figure 5b. Throughout the entire interval shown in Figure 5a, a band of cooler plasma, with ion temperature ~6 keV, moves earthward from 9 R_E to 6 R_E.

[20] As the main phase of the storm continues, second interval (Day 278, 1600 to Day 279, 0200 UT), there is a noticeable cooling of the plasma near the Earth on the nightside. A similar cooler region localized slightly postmidnight during storm main phase was also seen in the *Zaniewski et al.* [2006] remote ion temperature measurement analysis (keeping in mind that in this work, each *x* position includes premidnight and postmidnight ENA fluxes) and in analysis of years of in situ MPA measurements [*Denton et al.*, 2005]. Overall, both the dayside and nightside average ion temperatures decrease during this portion of the storm. There is an interesting region of increased ion temperature (highlighted by the white oval in Figure 3a) that begins around $x = -15\ R_E$ at 1840 UT and appears to propagate tailward to $x = -30\ R_E$ at 2200 UT until it can no longer be distinguished from the gradual increase in ion temperature that appears to originate in the deep tail and propagates toward the Earth. One possible explanation for this is a reconnection event occurring at $x = -15\ R_E$ that sent a jet of hot plasma, possibly a plasmoid, tailward. This event correlates with a large peak in the AL index (see Figure 4). Plasmoids have been observed to be created by reconnection at $x = -15\ R_E$, although our ion temperatures are higher and the tailward velocity much lower than the averages of 4.5 keV and 350–700 km/s, respectively, reported by *Ieda et al.* [1998]. However, plasmoids with slower or even stagnant velocities have been reported [*Moldwin and Hughes*, 1994].

[21] Increased ion temperatures originating in the deep tail and propagating earthward are more clearly seen in the third interval of Figure 3a (Day 279, 0640–1520 UT) starting at 0800 UT around $x = -53\ R_E$ and continuing until the data terminate at 1520 UT. The earthward trend of increased temperatures appears to be associated with a northward turning of B_z. After the rapid northward turning of B_z, the increased ion temperature "front" propagates toward the Earth at approximately 8–16 km/s, much slower than the 120 km/s flow of energetic ions in the magnetotail reported by *Baumjohann et al.* [1996]. If the ion heating

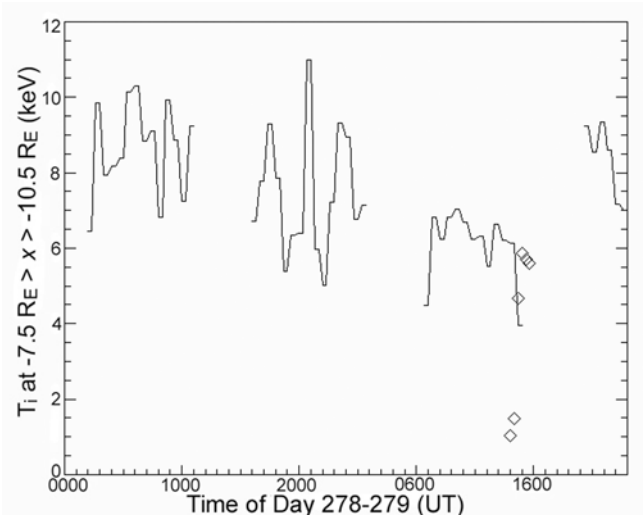

Figure 7. Ion temperatures calculated from MENA data (solid line) and measured by Geotail (diamonds). The row of temperatures used is indicated in Figure 3a by the blue box and corresponds to data taken at $-7.5\ R_E > x > -10.5\ R_E$.

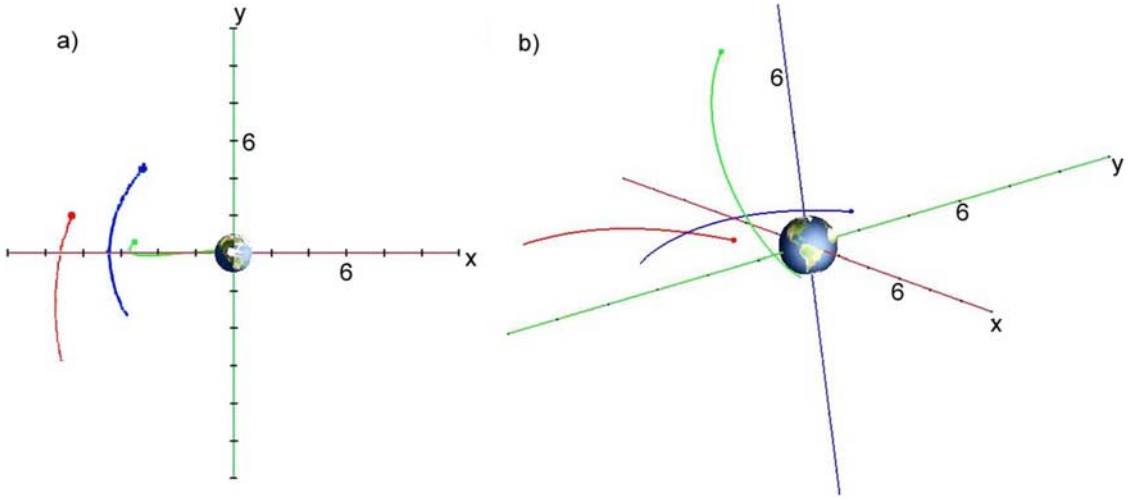

Figure 8. Orbit trajectories for 5 October 2000, 1400–1900 UT with (a) *xy*-plane (Sun to the right) and (b) perspective views for the Geotail (red), LANL geosynchronous (blue), and Imager for Magnetopause-to-Aurora Global Exploration (green) satellites. The dots indicate the satellite position at the beginning of the interval shown. (Plots made using SSCWeb 3D Orbit Viewer.)

"front" is associated with magnetotail reconnection, these data place the reconnection region well beyond the 20–30 R_E expected for a near-Earth neutral line (NENL). Therefore, these 1-D ion temperature images are consistent with either a much more distant neutral line or ion temperature increases resulting from convection of energetic ions up the tail and toward the Earth due to dipolarization of the magnetic field [*Delcourt et al.*, 1990].

[22] We note that these results are also consistent with previous single-point based studies of magnetotail ion heating. The measured ion temperatures are slightly larger than typical for the magnetotail [*Baumjohann et al.*, 2003], but since our averages include temperatures both before and after multiple substorms [*Horton et al.*, 2005], higher ion temperatures are expected [*Baumjohann et al.*, 1996].

[23] The agreement between the MPA in situ measurements and our remote measurements (Figure 6) is good. Significant changes in ion temperature (2–4 keV) on relatively short timescales (20–40 min) can be seen in both sets of data. While these variations are comparable to the errors in the remote temperature measurements, the agreement with the MPA data leads us to believe that at least some of the variation is real. Some of the observed variation may be evidence of the sawtooth oscillations of the periodic substorms [*Horton et al.*, 2005]. The clearest picture of this is seen in Figure 9 beginning at 1720 UT on 4 October with a large increase in ion temperature followed by oscillations until 0040 UT on 5 October. The onset of a substorm was observed by the FUV camera on IMAGE at 1720 UT [*Brandt et al.*, 2003]. The period of oscillation in our ion temperature measurements agrees with the ~2 h period typically observed in these periodic substorms [*Horton et al.*, 2005]. Some oscillation in the ion temperature during this interval can also be seen at other *x* axis locations (see Figures 6 and 7). That the ion heating by the substorm at 0600 UT was observed close to the Earth while ion heating from this substorm at 1720 UT was most evident further downtail agrees with the observation by *Brandt et al.* [2003] that the earlier substorm injected plasma onto closed drift trajectories while the later substorm injected plasma onto open drift trajectories due to an increase in the *y*-component of the electric field.

[24] While Geotail was only in the field of view for a short interval, the agreement between Geotail in situ measurements and our remote measurements (Figure 7) is also good. The measurements with the poorest agreement occur when Geotail was furthest from the *xy*-plane (see Figure 8b and note that the location of the spacecraft at the beginning of the interval is indicated by a dot) and therefore it was probably not in the central plasma sheet where the ion temperatures are highest (remember that our remote ion temperature measurements are weighted toward the hottest location along the line of sight).

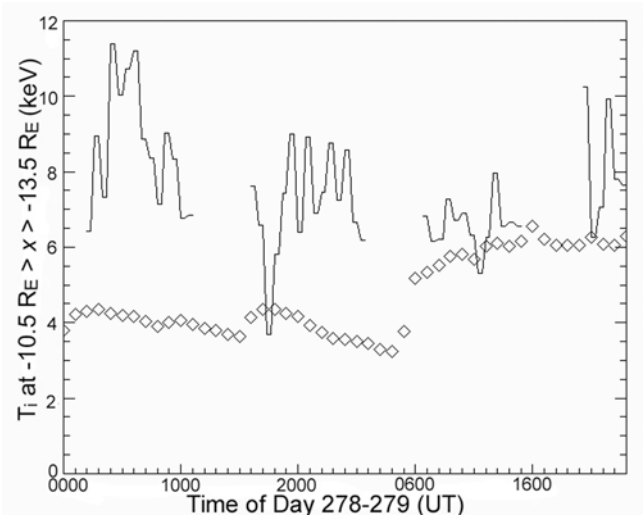

Figure 9. Ion temperatures calculated from MENA data (solid line) and calculated from the velocity of the solar wind (diamonds). The row of temperatures used is indicated in Figure 3a by the red box and corresponds to data taken at $-10.5\ R_E > x > -13.5\ R_E$.

[25] Our ion temperatures are in good agreement with the temperatures calculated using equation (1) (Figure 9) after 0600 UT on day 279 (end of main phase to early recovery phase). However, our measured ion temperatures are approximately twice as high as those calculated using equation (1) during the early portion of the storm main phase. Thus, the measurements indicate a plasma ion pressure that is three times higher than that used in the simulations. One explanation for the discrepancy is that the periodic substorms identified during day 278 could play a larger role in ion heating than the solar wind-forcing during the early portion of the storm main phase, i.e., the *Borovsky et al.* [1998] correlation fails during intervals of internally driven ion heating.

[26] The substantial difference between the downtail ion temperatures determined remotely from those predicted by solar wind correlative studies suggests that accurate modeling of storms cannot be accomplished through the use of such statistically based predictive expressions. This is particularly true during intervals of substorm activity when the solar wind does not play a significant role in the determination of the magnetotail ion temperature. The temporally and spatially resolved ion temperatures presented here should provide more realistic boundary conditions for such computational models.

5. Summary

[27] We have presented temporally and spatially resolved remote ion temperature measurements of the magnetosphere, including the magnetotail out to $x = -60\ R_E$. The measurements are calculated from MENA data taken during the first 48 h of the geomagnetic storm that occurred on 4–7 October 2000. The ion temperatures agree well with in situ measurements from multiple spacecraft. The characteristic heating and cooling of the magnetosphere throughout the phases of the storm agree with previous studies. Evidence of ion heating due to substorm activity is observed for two substorms, one during the early main phase and one during the late main phase of the storm. Both earthward and tailward flows of hot ions were observed, possibly indicating occurrences of magnetic reconnection in the magnetotail. We have found that our ion temperatures only agree with those calculated using a solar wind velocity scaling after the occurrence of a second ICME which coincided with the recovery phase of the storm. Our temperatures were 2–3 times higher during the main phase of the storm, indicating that the solar wind was not the primary driver of ion heating in the magnetotail during that phase. Rather, the occurrence of multiple periodic substorms likely dominated the magnetospheric dynamics. Because this solar wind velocity scaling is used to create boundary conditions for magnetospheric modeling, using ion temperatures calculated with the method reported here should yield more accurate models, potentially revealing important physical processes that occur during the main phase of geomagnetic storms.

[28] **Acknowledgments.** The work of E.E.S. and A.M.K was supported by subcontract from the Southwest Research Institute through NASA Prime contract NAS5–01095. The work of M. B. M. was supported by NSF grant ATM-0348398. The authors would like to acknowledge M. Thomsen, L. Frank, and D. J. McComas for providing the MPA, Geotail, and ACE data, respectively. We thank the ACE Science Center for providing the ACE data through CDAWEB at NASA. We thank N. Papitashvili for providing solar wind data through OMNIWeb at NASA. We thank the World Data Center at Kyoto University for providing the AL index data. We thank NASA for supporting the IMAGE mission and all members of the IMAGE and MENA teams.

[29] Wolfgang Baumjohann thanks the reviewers for their assistance in evaluating this paper.

References

Bame, S. J., D. J. McComas, M. F. Thomsen, B. L. Barraclough, R. C. Elphic, J. P. Glore, J. T. Gosling, J. C. Chavez, E. P. Evans, and F. J. Wymer (1993), Magnetospheric plasma analyzer for spacecraft with constrained resources, *Rev. Sci. Instrum.*, *64*, 1026, doi:10.1063/1.1144173.

Baumjohann, W., Y. Kamide, and R. Nakamura (1996), Substorms, storms, and the near-Earth tail, *J. Geomagn. Geoelectr.*, *48*, 177.

Baumjohann, W., R. Nakamura, R. Schoedel, and K. Dierschke (2003), Substorms, storms, and the storm-time plasma sheet, in *Disturbances in Geospace: The Storm-Substorm Relationship*, *Geophys. Monogr. Ser.*, vol. 142, edited by A. S. Sharma, Y. Kamide, and G. S. Lakhina, pp. 55–58, AGU, Washington, D. C.

Borovsky, J. E., M. F. Thomsen, and R. C. Elphic (1998), The driving of the plasma sheet by the solar wind, *J. Geophys. Res.*, *103*(A8), 17617, doi:10.1029/97JA02986.

Brandt, P., R. Demajistre, E. C. Roelof, S. Ohtani, D. G. Mitchell, and S. Mende (2002), IMAGE/high-energy energetic neutral atom: Global energetic neutral atom imaging of the plasma sheet and ring current during substorms, *J. Geophys. Res.*, *107*(A12), 1454, doi:10.1029/2002JA009307.

Brandt, P., D. G. Mitchell, S. Ohtani, R. Demajistre, E. C. Roelof, J.-M. Jahn, C. J. Pollock, and E. G. D. Reeves (2003), Storm-substorm relationships during the 4 October, 2000 storm. IMAGE global ENA imaging results, in *Disturbances in Geospace: The Storm-Substorm Relationship*, *Geophys. Monogr. Ser.*, vol. 142, edited by A. S. Sharma, Y. Kamide, and G. S. Lakhina, pp. 103–118, AGU, Washington, D. C.

Burch, J. L. (2000), IMAGE mission overview, *Space Sci. Rev.*, *91*, 1, doi:10.1023/A:1005245323115.

Delcourt, D., J. Sauvaud, and A. Pedersen (1990), Dynamics of single-particle orbits during substorm expansion phase, *J. Geophys. Res.*, *95*(A12), 20,853, doi:10.1029/JA095iA12p20853.

Denton, M. H., M. F. Thomsen, H. Korth, S. Lynch, J. C. Zhang, and M. W. Liemohn (2005), Bulk plasma properties at geosynchronous orbit, *J. Geophys. Res.*, *110*, A07223, doi:10.1029/2004JA010861.

Fok, M.-C., et al. (2003), Global ENA image simulations, *Space Sci. Rev.*, *109*, 77, doi:10.1023/B:SPAC.0000007514.56380.fd.

Henderson, M. G., M. F. Thomsen, R. Skoug, M. H. Denton, R. Harper, H. O. Funsten, and C. J. Pollock (2005), Calculation of IMAGE/MENA geometric factors and conversion of images to units of integral and differential flux, *Rev. Sci. Instrum.*, *76*, 043303-1.

Horton, W., E. Spencer, I. Doxas, and J. Kozyra (2005), Analysis of the October 3–7 2000 GEM storm with the WINDMI model, *Geophys. Res. Lett.*, *32*, L22102, doi:10.1029/2005GL023515.

Hoshino, M. (2005), Stratified current sheet during plasma sheet thinning, in *Frontiers in Magnetospheric Plasma Physics: Celebrating 10 Years of Geotail Operation*, edited by M. Hoshino, Y. Omura, and L. J. Lanzerotti, pp. 108–112, Elsevier, Oxford, U. K.

Hughes, W. J. (1995), The magnetopause, magnetotail, and magnetic reconnection, in *Introduction to Space Physics*, edited by M. G. Kivelson and C. T. Russell, pp. 227–287, Cambridge Univ. Press, New York.

Ieda, A., S. Machida, T. Mukai, Y. Saito, T. Yamamoto, A. Nishida, T. Terasawa, and S. Kokubun (1998), Statistical analysis of the plasmoid evolution with Geotail observations, *J. Geophys. Res.*, *103*(A3), 4453, doi:10.1029/97JA03240.

Kamide, Y., et al. (1998), Current understanding of magnetic storms: Storm-substorm relationships, *J. Geophys. Res.*, *103*(A8), 17,705, doi:10.1029/98JA01426.

Kaufmann, R., B. Ball, W. Paterson, and L. Frank (2001), Plasma sheet thickness and electric currents, *J. Geophys. Res.*, *106*(A4), 6179, doi:10.1029/2000JA000284.

Lin, Y., and D. W. Swift (1996), A two-dimensional hybrid simulation of the magnetotail reconnection layer, *J. Geophys. Res.*, *101*(A9), 19,859, doi:10.1029/96JA01457.

Liu, W. W., and G. Rostoker (1995), Energetic ring current particles generated by recurring substorm cycles, *J. Geophys. Res.*, *100*(A11), 21,897, doi:10.1029/95JA01934.

Lui, A. T. Y. (2005), Kinetic instabilities in a thin current sheet, in *Frontiers in Magnetospheric Plasma Physics: Celebrating 10 Years of Geotail Operation*, edited by M. Hoshino, Y. Omura, and L. J. Lanzerotti, pp. 113–122, Elsevier, Oxford, U. K.

McComas, D. J., P. Valek, J. L. Burch, C. J. Pollock, R. M. Skoug, and M. F. Thomsen (2002), Filling and emptying of the plasma sheet: Remote observations with 1–70 keV energetic neutral atoms, *Geophys. Res. Lett.*, *29*(22), 2079, doi:10.1029/2002GL016153.

Moldwin, M., and W. Hughes (1994), Observations of earthward and tailward propagating flux rope plasmoids: Expanding the plasmoid model of geomagnetic substorms, *J. Geophys. Res.*, *99*(A1), 183, doi:10.1029/93JA02102.

Moore, K. R., E. E. Scime, H. O. Funsten, D. J. McComas, and M. F. Thomsen (1994), Low-energy neutral atom emission from the Earth's magnetosphere, *Opt. Eng.*, *33*, 1–342, doi:10.1117/12.155924.

Nagai, T., M. Fujimoto, Y. Saito, S. Machida, T. Terasawa, R. Nakamura, T. Yamamoto, T. Mukai, A. Nishida, and S. Kokubun (1998), Structure and dynamics of magnetic reconnection for substorm onsets with Geotail observations, *J. Geophys. Res.*, *103*(A3), 4419, doi:10.1029/97JA02190.

Nosé, M., R. W. McEntire, and S. P. Christon (2005), Influence of solar wind on source of ring current plasma, in *Frontiers in Magnetospheric Plasma Physics: Celebrating 10 Years of Geotail Operation*, edited by M. Hoshino, Y. Omura, and L. J. Lanzerotti, pp. 48–53, Elsevier, Oxford, U. K.

Pollock, C. J., et al. (2000), Medium Energy Neutral Atom (MENA) imager for the IMAGE Mission, *Space Sci. Rev.*, *91*, 113, doi:10.1023/A:1005259324933.

Russell, C. T. (1990), The magnetopause, in *Physics of Magnetic Flux Ropes*, *Geophys. Monogr. Ser.*, vol. 58, edited by C. T. Russell, E. R. Priest, and L. C. Lee, pp. 439–453, AGU, Washington, D. C.

Scime, E. E., C. Pollock, J.-M. Jahn, J. Kline, and A. Keesee (2002), Ion heating in the terrestrial magnetosphere during substorms and storm-time: Medium energy neutral atom (MENA) observations, *Geophys. Res. Lett.*, *29*(10), 1438, doi:10.1029/2001GL013994.

Suszcynsky, D., J. Gosling, and M. Thomsen (1993), Ion Temperature Profiles in the Horns of the Plasma Sheet, *J. Geophys. Res.*, *98*(A1), 257, doi:10.1029/92JA01733.

Taktakishvili, A. L., A. Greco, P. Veltri, G. Zimbardo, L. M. Zelenyi, and A. Milovanov (2001), Magnetic turbulence and ion dynamics in the magnetotail, in *Physics of Space: Growth Points and Problems. Second "Rencontres de l'Observatoire," 10–14 Jan. 2000, Astrophysics and Space Science*, pp. 71–79, Kluwer Acad., Meudon, France.

Tsyganenko, N. A., and T. Mukai (2003), Tail plasma sheet models derived from Geotail particle data, *J. Geophys. Res.*, *108*(A3), 1136, doi:10.1029/2002JA009707.

Tsyganenko, N. A., and D. P. Stern (1996), Modeling the global magnetic field of the large-scale Birkeland current systems, *J. Geophys. Res.*, *101*(A12), 27187, doi:10.1029/96JA02735.

Veltri, P., G. Zimbardo, A. L. Taktakishvili, and L. M. Zelenyi (1998), Effect of magnetic turbulence on the ion dynamics in the distant magnetotail, *J. Geophys. Res.*, *103*(A7), 14,897, doi:10.1029/98JA00211.

Zaniewski, A. M., X. Sun, A. Gripper, E. E. Scime, J.-M. Jahn, and C. J. Pollock (2006), Evolution of remotely measured inner magnetospheric ion temperatures during a geomagnetic storm, *J. Geophys. Res.*, *111*, A10221, doi:10.1029/2006JA011769.

Zhang, J., K. P. Dere, R. A. Howard, and V. Bothmer (2003), Identification of solar sources of major geomagnetic storms between 1996 and 2000, *Astrophys. J.*, *582*, 520, doi:10.1086/344611.

Zhang, X. X., J. D. Perez, T. Chen, C. Wang, P. C. Brandt, D. B. Mitchell, and Y. L. Wang (2005), Proton temperatures in the ring current from ENA images and in situ measurements, *Geophys. Res. Lett.*, *32*, L16101, doi:10.1029/2005GL023481.

A. M. Keesee and E. Scime, Department of Physics, West Virginia University, Box 6315, Morgantown, WV 26506, USA. (ams_510@yahoo.com)

M. B. Moldwin, Institute of Geophysics and Planetary Physics, University of California, P.O. Box 951567, Los Angeles, CA 90095, USA.